Journal of Applied Polymer Science

Wet-Spun, Photoinitiator-Modified Polyacrylonitrile Precursor Fibers: UV-Assisted Stabilization

Marlon S. Morales, Amod A. Ogale
Department of Chemical Engineering, and Center for Advanced Engineering Fibers and Films, Earle Hall, Clemson University, Clemson, South Carolina 29634-0910
Correspondence to: Amod A. Ogale (E-mail: ogale@clemson.edu)

ABSTRACT: The role of dilute concentrations (~1 wt %) of a photoinitiator, 4,4′-bis(diethylamino)benzophenone, on the processability and properties of the resulting wet-spun polyacrylonitrile (PAN) fibers are reported. Rheology measurements show no adverse effect on the viscosities of solutions by the addition of the photoinitiator. Fibers containing photoinitiator were successfully wet-spun from PAN–DMSO solution. FTIR results prove that 4,4′-bis(diethylamino)benzophenone was retained in the fibers after coagulation and post-stretching. SEM micrographs show no deterioration of the post-stretched fiber microstructure due to the presence of photoinitiator. Tensile testing results show a small reduction in the strain-at-break of post-stretched fibers containing photoinitiator when compared with pure (control) PAN fibers. After UV treatment, fibers with 4,4′-bis(diethylamino)benzophenone display a higher tensile modulus compared with the other sets. Wide-angle X-ray diffraction results show no significant decrease in interplanar spacing and size of the crystals within the fibers containing photoinitiator, but such fibers retain a higher extent of molecular orientation after being UV treated. Conversion indices were measured from the WAXD spectra and compared with conventional thermal stabilized fibers. This correlation confirms that the addition of 1 wt % photoinitiator to PAN followed by 5 min of UV treatment leads to a conversion index that is observed in control fibers after more than an hour, which could reduce the conventional thermo-oxidative stabilization time significantly. These results indicate the potential of the dual stabilization route in generating precursor fibers with higher molecular orientation, and possibly reducing the thermo-oxidation time during carbon fiber processing. © 2013 Wiley Periodicals, Inc. J. Appl. Polym. Sci. 130: 2494–2503, 2013

KEYWORDS: fibers; properties and characterization; crosslinking; X-ray; rheology

Received 21 January 2013; accepted 16 April 2013; Published online 27 May 2013
DOI: 10.1002/app.39442

INTRODUCTION

High strength carbon fibers used in structural composites for aerospace applications are derived from solution-spun PAN precursor fibers.[1–5] However, the higher cost of carbon fibers compared with other reinforcing materials (viz. glass fibers) limits their use for the high-end applications where strength-to-density ratio is critical.[4–8] The demand for carbon fibers is expected to grow to about 150,000 metric tons over the next decade from current demand of 40,000 metric tons. However, a large fraction of the increase is anticipated in the industrial sector that is cost-sensitive.[5,9] For cost effective products, such as automotive application, there is a need for the development of novel processes and precursors to reduce the carbon fiber production cost and expand the use of carbon fibers.

For the conversion of PAN into carbon fibers, thermal oxidative stabilization and carbonization steps have to be conducted.[4,10,11] The thermal stabilization process is believed to be the most important step during the carbon fiber manufacture, because the conditions employed during stabilization will dictate most of the final carbon fiber properties.[12–15] Also, thermal stabilization is the rate-limiting step in the production of PAN-based carbon fibers.[3,16] During thermo-oxidative stabilization, heat is produced by exothermic reactions and a temperature gradient is generated within the fiber due to the low thermal conductivity of PAN precursors (~0.26 W m^{-1} K^{-1}).[3,4,10,17,18] The dissipation of this energy is very important and the energy generation can be controlled by using slow heating rates during the thermal stabilization of the fibers.[16,19,20] Simultaneously, post-drawing of fibers must be performed to collapse the voids and to increase molecular orientation.[11,21,22] However, this orientation is partly lost due to molecular relaxation processes that occur when the PAN precursor fibers are heated up to 300°C during the stabilization step. Additional stresses must be applied during stabilization and carbonization steps in an attempt to regain the molecular orientation. This strategy results in carbon fibers with high strength, but the limited molecular orientation prevents the fibers from developing an ultra high modulus.[14,15,18,23]

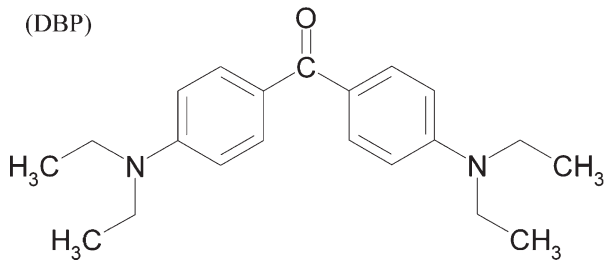

Figure 1. 4,4′-Bis(diethylamino)benzophenone (BDP) used throughout this study.

PAN based terpolymer containing a photo sensitive comonomer, such as acryloyl benzophenone, have been investigated and successfully converted into carbon fibers in previous studies.[8,24] In addition, polymerization and stabilization reactions are known to proceed faster and at lower temperatures when initiated by UV radiation.[24–26] In a recent study, on solution-cast PAN films, we established that it is possible to start cyclization and crosslinking reactions associated with thermal stabilization at lower temperatures by the addition of small amounts (1 wt %) of photoinitiator. Subsequent UV exposure at lower temperatures leaded to a reduction of the conventional thermal stabilization time.[27] However, the role of external photoinitiator added to the polymer solution prior to wet-spinning (i.e., without synthesizing the photoinitiator into the polymer chain itself) on the rheology of the PAN-dope, wet-spinnability, and characterization of precursor fibers remain unaddressed.

Therefore, the overall goal of this research was to study the effect of the addition of photoinitiator and further UV exposure on the properties of the resulting PAN and pre-stabilized fibers. The addition of photoinitiator and further UV treatment is investigated here as an alternative to reduce the thermal stabilization processing time while keeping the properties of resulting fibers. Alternatively, this strategy may lead to modifications in the mechanisms of the cyclization and crosslinking reactions that can lead to enhanced properties of carbon fibers.

EXPERIMENTAL

Materials

Polyacrylonitrile homopolymer with a molecular weight (M_w) of 233,000 and a glass transition temperature (T_g) of 125°C was used throughout this study. This PAN homopolymer was obtained from Scientific Polymer (Ontario, NY). The photoinitiator used throughout this study, 4,4′-bis(diethylamino)-benzophenone (BDP), is shown in Figure 1. This photoinitiator generates free radicals by hydrogen abstraction and has UV absorbance peak at 378 nm in the UVA region (320–390 nm).[28,29] The solvent used in this study was dimethyl sulfoxide (DMSO) with a density of 1.1 g cm^{-3} and viscosity of 0.002 Pa s (both measured at 25°C). Both, photoinitiator and solvent were obtained from Sigma-Aldrich (Aldrich Chemical Company, Milwaukee, WI). Also a standard silicon powder reference material was used for line position and line shape during X-ray diffraction studies (NIST reference material® 640d). All materials were used as received.

Fiber Spinning

PAN-based precursor and photoinitiator (where applicable) were dissolved in a 99 : 1 mass ratio in DMSO at 70°C. The amount of solids in solution was kept at ~16 wt %. Fibers were spun from solution using a custom-built wet-spinning unit fitted with a spinnerette that had 100 holes each one with an approximate diameter of 68 μm. A volumetric flow of 0.6 mL min^{-1} was maintained during the spinning of the fibers. The coagulation bath consisted of 70 wt % DMSO/30 wt % distilled-deionized water. After the coagulation bath, the solidified fibers were passed through a distilled-deionized water washing bath; both baths were kept at ~20°C. The effective length of the coagulation and washing bath were 40 and 80 cm, respectively. The rolls of fibers were placed in an oven and dried at 70°C for about 24 h. Next, the fibers were post-stretched in a distilled-deionized water bath at approximately 80°C. The effective length of the post-stretching bath was 80 cm. Pure PAN fibers as well as fibers containing 1 wt % of photoinitiator were thus produced.

UV-Treatment of Samples

The fibers were irradiated with a Nordson 4.5 kW UV curing lamp (Model 111465A). Two different UV sources were used: mercury (model PM1163) and iron halide (model PM1163F) bulb. The intensity of both bulbs was measured using a high energy UV radiometer (model PP2000, Electronic Instrumentation and Technology). For the mercury bulb intensity values of approximately 0.228, 0.196, 0.032, and 0.095 W cm^{-2} were measured for the UVA, UVB, UVC, and UVV ranges, respectively. The intensity values measured from the iron-halide bulb were approximately 0.378, 0.131, 0.014, and 0.236 W cm^{-2} for the UVA, UVB, UVC, and UVV ranges, respectively. Mercury bulbs are the most widely used UV source and they provide a broadband output distribution in the four UV regions.[26,30] Iron halide bulbs have the feature of possessing a higher energy emission in the UVA region. As noted earlier, the photoinitiator BDP has a UV absorption peak at 378 nm (UVA). Thus, by choosing an appropriate UV source (mercury vs. iron halide), it may be possible to control the interactions between the UV radiation and the PAN-based precursor or photoinitiator. Besides cyclization, dehydrogenation, and crosslinking, UV radiation acting directly on the PAN precursor leads to chain scission as well, which hinders the stabilization reaction and affects the properties of the resulting fibers.[27] Iron halide reduces the amount of energy delivered in the UVC and UVB regions that interact with PAN-based precursors (UV absorption peak at ~274 nm) and delivers more energy in the UVA region where the UV absorption peak of the photoinitiator is located. As shown later, the UV profile of the UV source selected will influence the rate of stabilization reaction, and thence, the properties of the material for a given UV treatment time.

Segments of approximately 10 inches (matching effective length of UV bulbs) were irradiated for 300 s at approximately 150°C. The bundle of fibers was held under approximately 0.1 g

denier^{-1} of tension during the UV treatment. The distance between the samples and the UV source was kept constant at approximately 20 cm. A custom-made air cooling system was placed inside the UV chamber to remove the excess of heat generated by the source during the UV-treatment and control the temperature inside the UV chamber. All UV treated samples were compared against two types of control fibers. The first control consisted of pure as-produced PAN fibers. The second control consisted of fibers that were covered by a metal sheet (to avoid UV exposure) but ones that were treated in the same UV chamber to provide similar thermal exposure as that received by UV treated samples (that also experienced the slightly elevated temperatures).

Finally, PAN fibers were only thermo-oxidative stabilized (as in conventional processes) to produce control samples whose extent of cyclization could be compared with those of the UV treated samples. The samples were stabilized under tension (0.1 g denier^{-1} below 200°C and 0.05 g denier^{-1} above 200°C), heated at 2.5°C min^{-1} to 300°C, and held there for 30 min. During this thermal oxidation, samples were removed from the oven at 150, 175, 200, 225, 250, 275, 300, and 300°C (after 30 min) to analyze and quantify the partial extent of the cyclization reaction.

Characterization

To determine the flow characteristics of the PAN-dopes, the solutions were tested for their rheological response using an ARES LS0012701 advanced rheometer with a cone-and-plate fixture for small shear rates (0.1–30 s^{-1}) and an ACER 2000 capillary rheometer for high shear rates (30–30,000 s^{-1}). The cone-and-plate fixture had a diameter of 25 mm and a cone angle of 0.1 rad. The capillary employed during the experiments had a "L/D" value of 30. All testing was conducted at room temperature (~25°C). The viscosities values for each solution were fitted using the generalized Newtonian or Carreau model [eq. (1)]. Where $\eta(\dot{\gamma})$ is the predicted shear viscosity, $\dot{\gamma}$ is the shear rate, λ is the time constant, η_0 is the zero shear rate viscosity, η_∞ is the infinite shear rate viscosity, and n corresponds to the power law index. For polymer solutions, the solvent viscosity is usually used for the η_∞ parameter.[31,32]

$$\frac{\eta(\dot{\gamma})-\eta_\infty}{\eta_0-\eta_\infty}=[1+(\lambda\dot{\gamma})^2]^{(n-1)/2} \quad (1)$$

Fourier transform infrared spectroscopy (Nexus 870 FT-IR ESP, Nicolet) was used to confirm the presence of photoinitiator in the fibers after being wet-spun and post stretched in hot water. The scans were conducted from 400 to 4000 cm^{-1} and the transmittance intensities were normalized against the intensity of the 2940 cm^{-1} peak (CH_2 asymmetric stretching) for comparison.

Morphological analysis of fibers was conducted by scanning electron microscopy with a Mitsubishi 4800 SEM unit. To retain the cross section shape and other physical features of the fibers, the fibers were submerged into liquid nitrogen for approximately 1 min and later broken. To determine the effective diameter of the fibers (with and without photoinitiator) Image-Pro Plus 7.0 (Media Cybernetics) analysis software was used to measure the cross section area of each type of sample and the effective diameter calculated from these area measurements. At least 40 cross section areas were measured for each type of fiber.

A PHOENIX single filament tensile testing unit (Measurements Technology) was used to measure the mechanical properties of the different fibers types produced along this study. The single fibers were mounted on 25 mm paper tabs. At least 20 samples per type of fibers were prepared and tested.

Wide angle X-ray diffraction (WAXD) analysis was conducted on bundles of fibers using a Rigaku-MSC (Houston, TX) X-ray diffraction unit. The X-ray diffraction pattern was captured through image plate and the analysis of WAXD generated images were analyzed using Polar v2.6.7 (Stonybrook Technology and Applied Research, STAR). The curve fitting of the spectra was done using OriginPro 7 (v7.0383, OriginLab Corporation). The unit generates an X-ray beam with a wavelength of 1.5406 Å (Cu target). The diameter of the X-ray beam hitting the sample was ~0.5 mm. The distances between the X-ray source and sample and the sample and the image plate detector were approximately 70 and 12 cm, respectively. Operation conditions of the X-ray source were 45 kV and 0.65 mA. The gas used for most of the beam path was helium. Each bundle of fibers was mounted on a 10 mm paper tab and sprinkled with silicon standard powder. The exposure time per sample was approximately 2 h.

The crystal plane spacing was calculated using Bragg law and lattice geometry equation for hexagonal crystal structure observed in PAN. The crystal size was calculated using Scherrer formula. Warren's broadening correction was used to correct the system broadening on each WAXD scan.[33–40] Also, conversion or aromatization indices (CI) were determined using the following equation[37,41,42]:

$$\text{Conversion index}(\%)=\frac{A_A}{A_A+A_P}\times 100\% \quad (2)$$

Where A_A is the area of the peak associated with the aromatic structure around $2\theta = 25°$ and A_p correspond to the area of the (100) crystal peak of PAN at $2\theta = 17°$. In addition, the Rigaku-MSC diffractometer is capable of measuring the orientation of the crystal in the fibers. These azimuthal scans were conducted on the most prominent peak of the PAN spectra, which is the (1 0 0) peak.

RESULTS AND DISCUSSION

Spinning of Fibers Containing Photoinitiator

Figure 2 displays steady shear viscosity versus shear rate results for PAN solutions with and without BDP. The open symbols represent the viscosity values measured at lower shear rates (0.1–30 s^{-1}) using the cone-and-plate fixture. The solid symbols correspond to the viscosity values measured at higher shear rates (30–30,000 s^{-1}) using the capillary rheometer. Both types of solutions displayed a shear-thinning behavior at high shear rates with an approach to Newtonian plateau at shear rates less than about 0.5 s^{-1}. The Carreau model was used to fit the viscosity data. For pure and BDP containing dopes, power law indices of 0.558 ± 0.028 and 0.544 ± 0.011, time constants of 1.85 ± 0.78 and 1.54 ± 0.35 s, and zero shear rate viscosity of

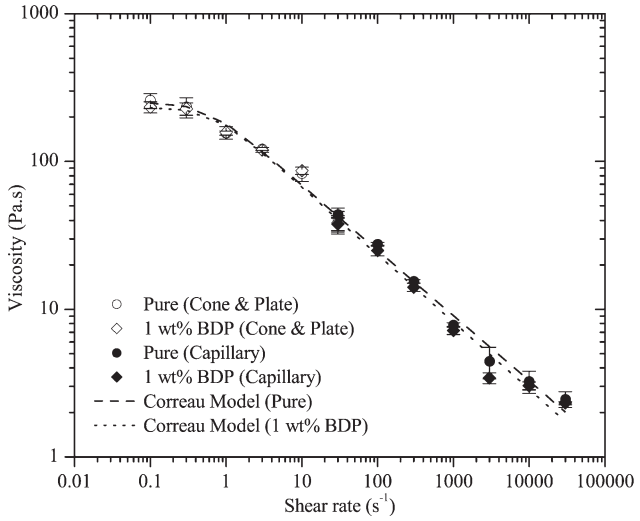

Figure 2. Viscosity versus shear rate results for PAN solutions with and without photoinitiator (at ~25°C).

250 ± 34 and 232 ± 8 Pa s, respectively, were obtained. At 95% confidence, the presence of photoinitiator in the solution did not significantly affect the viscosity of the dope. Thus, the presence of photoinitiator has no adverse effect on the viscosity of the dopes. This observation was generally consistent with the fact that the concentration of BDP in the actual solution was small (~0.16 wt %).

All wet-spinning experiments were conducted at room temperature (~25°C). During the spinning of both types of fibers, the total amount of solids in solution was hold at about 16 wt %. Higher dope concentrations (17–21 wt %) were difficult to spin on a continuous basis for both types. A linear take up velocity of 190 cm min^{-1} was employed during the spinning of the fibers. The drawing ratio was kept in between 1.15 and 1.2. The drawing ratio used during the post-stretching step was approximately 3. Higher drawing ratios led to fiber breakage during spinning and post-stretching. Pure PAN fibers as well as fibers containing 1 wt % of photoinitiator were successfully produced.

Figure 3 displays representative SEM micrographs of as-produced PAN fibers. Figures 3(a) and (b) correspond to pure PAN fibers and those containing 1 wt % BDP, respectively. Both types of fibers show the characteristic kidney shape of wet-spun PAN-based fibers.[5,11,21,36,38] No noticeable deterioration or change in the microstructure of the fibers containing photoinitiator was observed when compared with pure control fibers. Thus, the presence of photoinitiator does not significantly affect the morphology of the fibers. The diameters of pure and 1 wt % BDP–PAN fibers were 11.9 ± 0.3 and 11.4 ± 0.3 μm, respectively. At 95% confidence level, there was no significant difference between the effective diameters of the pure fibers and the fibers containing 1 wt % BDP.

To identify the presence of photoinitiator in the fibers after spinning and post-stretching, FTIR analysis was conducted on pure and 1 wt % BDP post-stretched fibers. Figure 4 shows the comparison between the FTIR spectra of the pure and 1 wt % BDP fibers. The peaks located at 2940, 2865, 2242, 1454, and

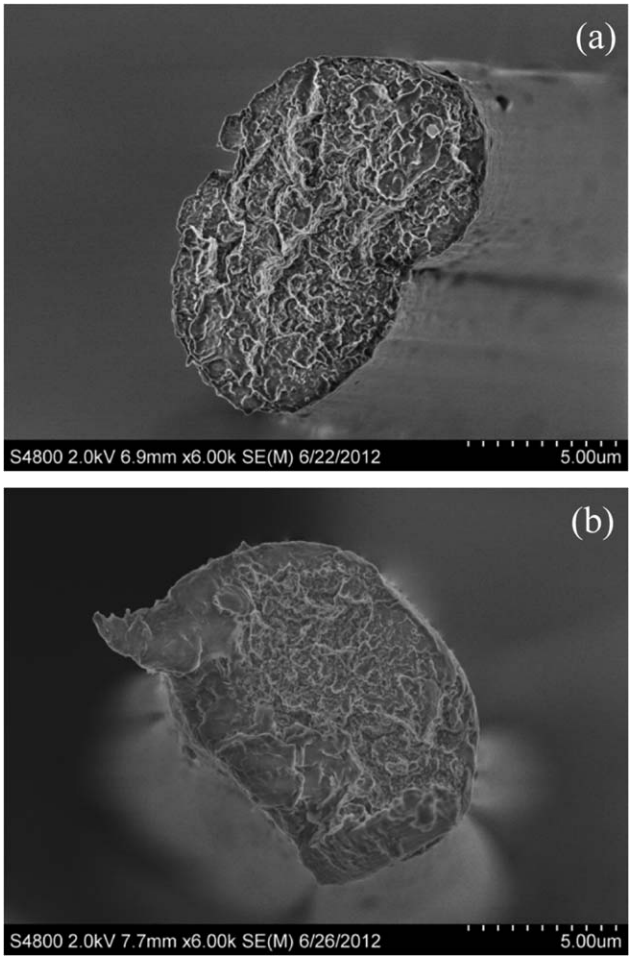

Figure 3. Representative SEM micrographs of as produced PAN fibers: (a) pure PAN fibers, (b) fibers containing 1 wt % BDP.

1055 cm^{-1} have been assigned to CH_2 asymmetric stretching, CH_2 symmetric stretching, C≡N stretching, CH_2 scissor vibration, and –C–C–C– backbone bending, respectively.[10,15,27,43,44]

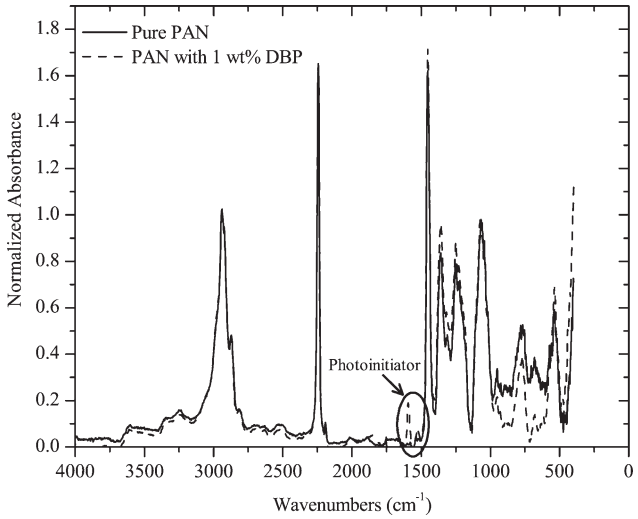

Figure 4. Comparison between FTIR results obtained from fibers to confirm the presence of photoinitiator.

Applied Polymer SCIENCE

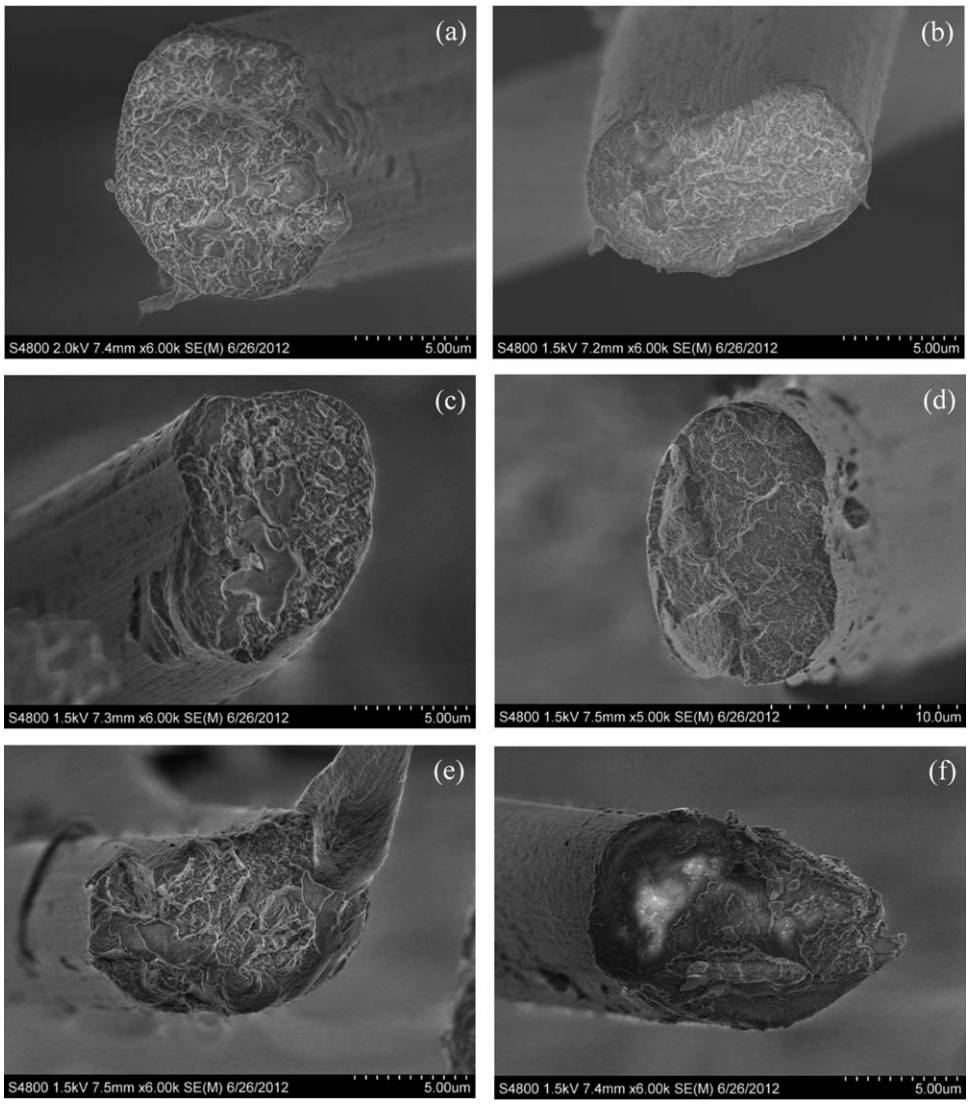

Figure 5. Representative SEM micrographs of PAN fibers with and without photoinitiator after being UV treated: (a) thermally exposed pure PAN fibers, (b) thermally exposed fibers containing 1 wt % BDP, (c) pure PAN fibers UV treated with iron halide bulb, (d) 1 wt % BDP PAN fibers UV treated with iron halide bulb, (e) pure PAN fibers UV treated with mercury bulb, and (f) 1 wt % BDP PAN fibers UV treated with mercury bulb.

The spectrum of the fibers containing 1 wt % DBP shows two extra peaks associated with the presence of photoinitiator in the fibers located at 1595 and 1525 cm^{-1}. The 1595 cm^{-1} peak has been assigned to the C=O stretching and the 1525 cm^{-1} to the C=C stretching (in ring), respectively. These two peaks are a proof of the presence of photoinitiator in the fibers after the spinning process. Thus, photoinitiator is retained in the fibers after coagulation and post-stretching despite the out-diffusion of the solvent during the coagulation stage.

Influence of UV Radiation

Figure 5 displays representative micrographs of control and active samples UV-treated either with a mercury or iron halide bulb. Figure 5(a) and (b) correspond to thermally exposed non-UV treated pure PAN fibers (control #1) and thermally exposed non-UV treated fibers containing 1 wt % BDP (control #2), respectively. Figure 5(c) and (d) are representative micrographs of pure and 1 wt % BDP–PAN fibers UV treated with the iron halide source, respectively. Figure 5(e) and (f) correspond to pure and 1 wt % BDP–PAN fibers UV treated with the mercury halide source, respectively. In all cases, the fibers retained the characteristic kidney shape of wet-spun PAN-based fibers.[5,11,21,36,38] At 95% confidence level, there was no significant difference between the effective diameters among the different samples. Another important observation is that the UV-treatment of the fibers did not lead to skin-core structure formation on any of the UV treated fibers. Skin-core structure is undesired during the stabilization of PAN-based fibers because leads to poor quality (mechanical properties of the) stabilized and carbonized fibers.[5,7,16,19,34,37]

Figure 6 shows representative tensile testing curves of each set of samples. Figure 6(a) corresponds to as-produced, thermally exposed, and UV treated with either iron halide or mercury bulb pure PAN fibers. Figure 6(b) shows the same treatment conditions but for fibers containing 1 wt % BDP. The limit of

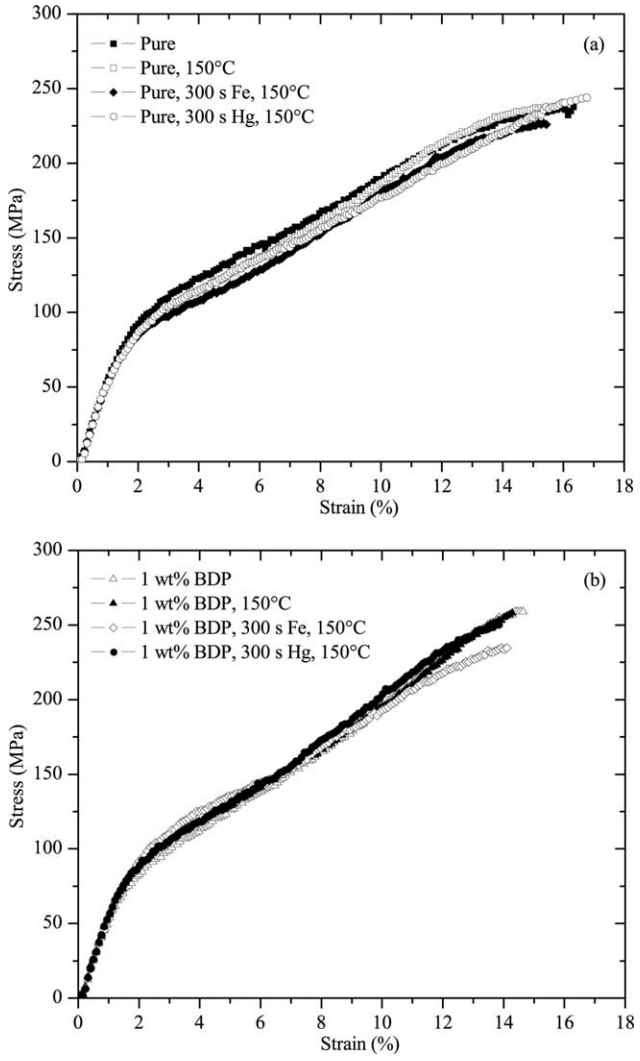

Figure 6. Representative tensile testing curves of each set of samples: (a) pure PAN, (b) PAN fibers containing 1% BDP.

linear proportionality was approximately 1% for all samples. Figure 6 also shows that the upper and lower yield points seem very close to the proportionality limit. Also, a small necking section is observed just before breakage. Table I summarizes the tensile testing results conducted on single filaments. These tensile properties of the PAN fibers are consistent with those reported in the literature: 10–25% for the breaking strain, 0.1–0.7 GPa for strength, and 1–10 GPa for tensile modulus.[1,7,8,12,14,18,42,45,46]

Tensile testing results shown in Table I indicate that, at 95% confidence, there is significant difference in the breaking strain between pure and 1 wt % BDP fibers; the presence of photoinitiator reduces the elongation capabilities of the fibers by ~1%. These results show no significant statistical differences, at 95% confidence, between the ultimate tensile strength among different specimens. On the other hand, at 95% confidence, the two set of fibers containing 1 wt % BDP UV treated for 300 s (5 min) with either mercury or iron halide displayed higher tensile modulus than the other set of samples. In addition, these tensile testing results show that fibers containing 1 wt % BDP UV

Table I. Single Filament Tensile Results with 95% Confidence Intervals

Sample	Tensile modulus (GPa)	Max stress (GPa)	Break strain (%)
Pure	7.0 ± 0.3	0.24 ± 0.01	16.4 ± 0.5
Pure, 150°C	7.1 ± 0.3	0.24 ± 0.01	14.9 ± 1.2
1 wt % BDP	7.0 ± 0.3	0.26 ± 0.01	14.3 ± 0.5
1 wt % BDP, 150°C	7.1 ± 0.4	0.25 ± 0.01	14.0 ± 0.8
Pure, 300 s Fe, 150°C	6.8 ± 0.3	0.22 ± 0.01	15.2 ± 1.4
Pure, 300 s Hg, 150°C	7.0 ± 0.3	0.24 ± 0.01	16.7 ± 0.5
1 wt % BDP, 300 s Fe, 150°C	7.5 ± 0.3	0.23 ± 0.01	13.5 ± 1.3
1 wt % BDP, 300 s Hg, 150°C	7.7 ± 0.2	0.25 ± 0.01	13.8 ± 0.8

treated with a mercury source exhibit the highest tensile modulus of all eight set of samples (significant at 95% confidence). This proves the combined positive effect of the addition of photoinitiator and 300 s of UV treatment on the fibers.

The higher tensile modulus shown by the 1 wt % BDP fibers UV treated with the mercury bulb compared with the same fibers UV treated with the iron halide bulb can be explained based on the differences in the spectral output of each type of bulb. Mercury bulbs deliver more energy in the UVC region and iron halide bulbs produce higher energy output in the UVA region (matching the UV absorption region of BDP). PAN has a UV absorption peak in the UVC region (~274 nm). Thus, the samples UV treated with the mercury bulb display a higher combined effect of the photoinitiator radicals, produced by the interaction of the photoinitiator with the UVA region, and UVC radiation directly interacting with the polymer chains. As mentioned earlier, the emission of UVC radiation is lower for iron halide bulbs compared with mercury bulbs. Therefore, the interaction between the radiation emitted by the iron halide bulb and the polymer chain is lower and the photoinitiator radicals are the ones that mainly interact with the polymer chains.[27] These results are very encouraging since the final mechanical properties of the carbon fibers depend greatly on the mechanical fibers of the precursor fibers.[2,6,10,21,22,35,38]

Figure 7 shows representative wide angle X-ray diffractograms of as-spun pure, post-stretched pure, and post-stretched with 1 wt % BDP PAN fibers. Integrated 2θ scans, displayed in Figure 7(a), show the first peak at ~17° corresponding to the (1 0 0) plane of the PAN precursor. The second peak corresponds to the combination of the amorphous halo at ~26° and the (1 1 0) plane peak of PAN at ~29.5°.[35–39,47–49] Silicon standard was added to each of the different fiber samples as a calibration standard. This silicon standard shows three sharp peaks at 28.44°, 47.3°, and 56.12° corresponding to its (1 1 1), (2 2 0), and (3 1 1) planes, respectively.

As noted before, the orientation of the crystals in the fibers was measured from the azimuthal scans conducted on the (1 0 0)

Applied Polymer SCIENCE

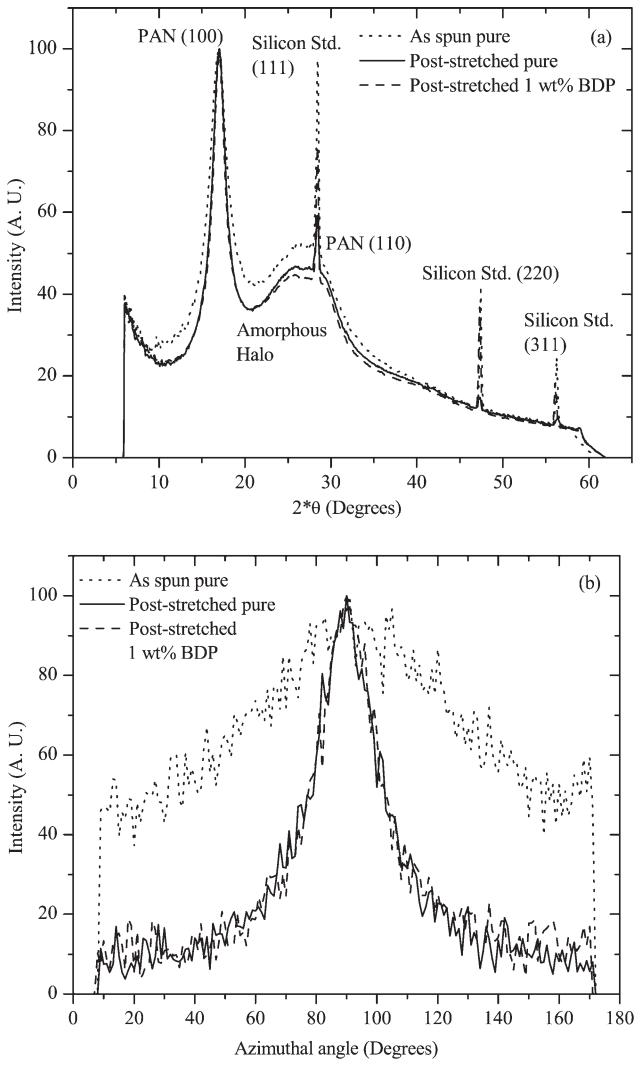

Figure 7. Representative WAXD result of as-spun and post-stretched PAN fibers: (a) integrated 2θ scan; (b) azimuthal scan of the PAN (1 0 0) peak.

peak of the PAN spectra. Figure 7(b) shows the azimuthal scans of (1 0 0) peak of as-spun pure, post-stretched pure, and post-stretched with 1 wt % BDP PAN fibers. Sharp azimuthal peaks for a given set of planes mean higher orientation, whereas, broad peaks indicate low orientation. As expected, post-stretched PAN fibers have significant higher orientation in comparison with that of as-spun fibers. Similar orientation is achieved for pure and 1 wt % BDP PAN fibers after being post-stretched. To compare the crystal orientation in the different set of fibers, the full-width-at-half-maximum (FWHM) was measured for each azimuthal scan. The smaller the FWHM value, the more oriented are the crystals within the fibers.

Table II summarizes the WAXD results obtained from all the different set of samples. After post-stretching, the interplanar spacing between the (1 0 0) plane was reduced and the orientation and crystal size was increased for pure and 1 wt % BDP-PAN fibers. Also, the results show no negative effects (at 95% confidence) for the interplanar spacing and size of the crystals within the fibers containing photoinitiator as compared with pure control fibers. In a previous study, it was shown that PAN-based precursors containing 1% BDP UV treated for 300 s show higher extents of cyclization reaction as compared with other set of samples.[27] Here, WAXD results show that during the UV treatment (cyclization reaction) these samples are able to retain their molecular orientation. This is not the case for pure UV treated samples. The retention of the orientation of the polymer chains within the fibers can lead to more polymer chains undergoing cyclization, leading to higher conversions. These results agree well with the tensile testing results that show superior mechanical properties for samples containing 1% BDP and UV treated for 300 s due to the fact that they are able to retain molecular orientation. For this system, higher molecular orientation leads to higher mechanical properties of the fibers.[10,15,18,21–23]

Figure 8 displays the WAXD spectra of pure PAN fibers at different stages during the traditional thermal stabilization in air. Figure 8(a) and (b) correspond to the integrated 2θ scan and the azimuthal scan of the PAN (1 0 0) peak, respectively. Table III summarizes the lattice parameters calculated from the spectra shown in Figure 8. Between room temperature and 150°C, the (1 0 0) peak becomes sharper and an increase in orientation and crystal size is observed in the fibers. Literature studies have discussed interesting effects of induced anisotropy due to the applied UV radiation.[50] However, as observed in the conventional thermal stabilized samples, most of the induced

Table II. WAXD Results with 95% Confidence Intervals

Sample ID	l_a (Å)	a (Å)	(1 0 0) FWHM (°)
Pure as spun	31.1 ± 3.2	6.048 ± 0.025	75.2 ± 2.5
1 wt % BDP as spun	29.4 ± 3.3	6.064 ± 0.029	75.8 ± 2.0
Pure after stretch	42.3 ± 1.9	6.001 ± 0.020	26.1 ± 0.9
1 wt % BDP after stretch	45.8 ± 2.2	6.019 ± 0.019	24.6 ± 1.4
Pure (150°C, NO UV, control)	41.8 ± 1.8	6.028 ± 0.038	28.3 ± 0.9
1 wt % BDP (150°C, NO UV, control)	42.4 ± 0.4	6.034 ± 0.015	25.3 ± 0.2
Pure, 300 s Fe UV, 150°C	43.8 ± 1.0	6.032 ± 0.010	29.8 ± 1.3
Pure, 300 s Hg UV, 150°C	43.6 ± 1.4	6.047 ± 0.025	29.7 ± 0.6
1 wt % BDP, 300 s Fe UV, 150°C	48.9 ± 4.9	6.029 ± 0.021	25.7 ± 1.8
1 wt % BDP, 300 s Hg UV, 150°C	46.3 ± 1.5	6.036 ± 0.016	25.6 ± 1.1

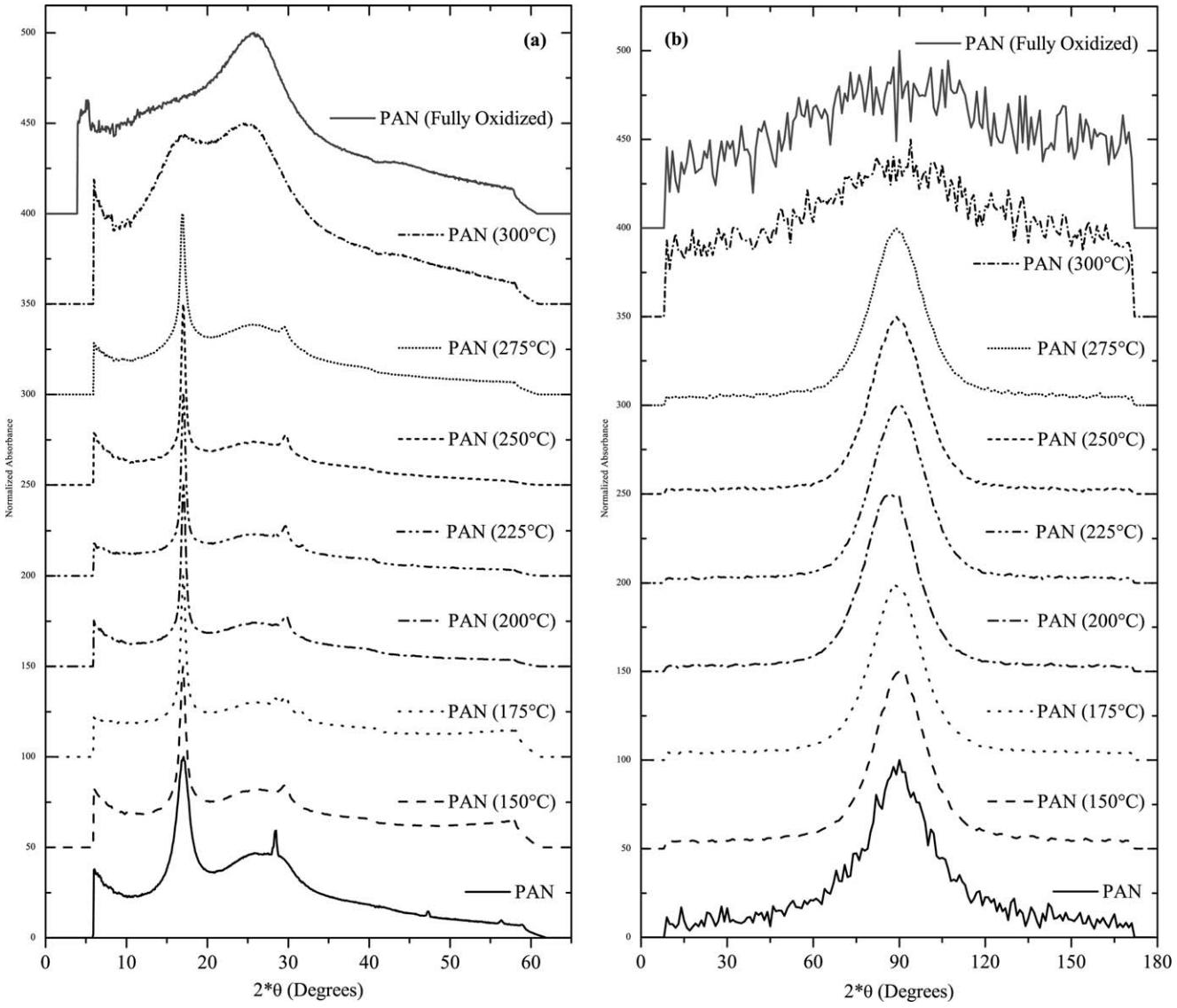

Figure 8. WAXD spectra of pure PAN fibers at different stages during traditional thermo-oxidative stabilization: (a) integrated 2θ scan; (b) azimuthal scan of the PAN (1 0 0) peak.

Table III. WAXD Results with 95% Confidence Intervals of Pure PAN Fibers at Different Stages During Traditional Thermal Stabilization in Air

Fiber temperature (°C)	l_a (Å)	a (Å)	(100) FWHM (°)	CI (%)
25	42 ± 2	6.001 ± 0.020	26.1 ± 0.9	1 ± 2
150	90 ± 2	6.025 ± 0.013	20.3 ± 1.1	1 ± 2
175	107 ± 2	6.012 ± 0.020	20.1 ± 0.9	2 ± 2
200	119 ± 2	6.001 ± 0.020	21.2 ± 1.0	2 ± 2
225	126 ± 4	6.003 ± 0.018	22.1 ± 0.9	1 ± 2
250	134 ± 4	6.009 ± 0.017	21.3 ± 0.9	16 ± 8
275	98 ± 2	6.040 ± 0.020	21.3 ± 1.2	37 ± 5
300	13 ± 1	6.198 ± 0.124	79.6 ± 5.5	52 ± 14
300 (after 30 min)	8 ± 1	6.576 ± 0.079	104.7 ± 4.4	64 ± 2
1 wt % BDP, 300 s Fe UV, 150°C	49 ± 5	6.029 ± 0.021	25.7 ± 1.8	8 ± 1
1 wt % BDP, 300 s Hg UV, 150°C	46 ± 2	6.036 ± 0.016	25.6 ± 1.1	14 ± 2

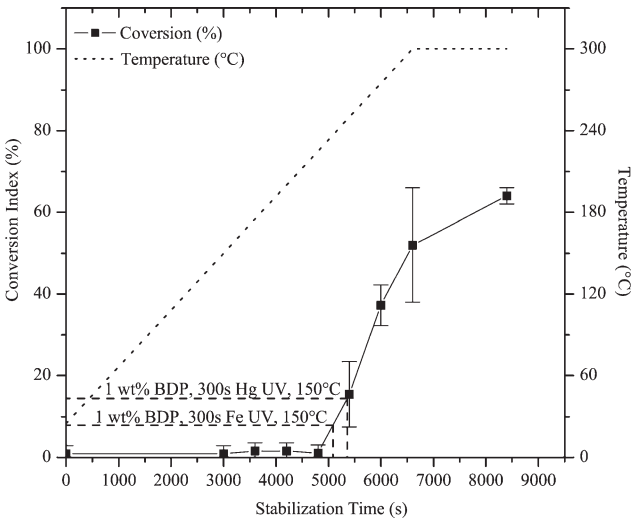

Figure 9. Correlation between stabilization temperature and conversion indices (with trend line) of pure PAN fibers during the thermal stabilization step.

anisotropy in the current samples can be attributed to the fact that the samples are under tension during processing.

Between 150 and 225°C, growth of the crystal size is mainly observed. At 225°C, dramatic changes are observed in the spectra. Between 225 and 250°C, the crystal size stops increasing, and around 250°C, the (1 0 0) PAN peak starts broadening and becomes weaker. This indicates an increment on the interplanar spacing and a reduction on the crystal size and orientation of the original PAN structure. In contrast, a strong aromatic peak starts to emerge. This evolution of structure is consistent with that reported in the literature.[15,37,41,46]

Based on WAXD spectra displayed in Figure 8, the conversion indices for pure, non-UV treated, thermally stabilized samples are presented in Figure 9 (Table III) as a function of the thermal stabilization time. Also included is the temperature profile followed during these thermal stabilization experiments. The dashed lines indicate the conversion indices of the samples containing 1 wt % DBP UV treated with mercury or iron halide UV source at 150°C for 300 s. The results show that 300 s (5 min) of UV treatment of the PAN-based precursor containing 1 wt % DBP are approximately equivalent to the first 5000 s (about 83 min) of the thermal oxidation process, i.e., a reduction of approximately half of the time needed for conventional stabilization process. This correlation between conversion index and processing time is consistent with that obtained from our previous study using FTIR spectra.[27] The other conversion indices for UV treated samples in the absence of photoinitiator were not statistically different from the initial indices for pure PAN samples thermally stabilized, and not included in the figure. These kinetic results indicate the potential for developing a novel and more rapid process for stabilization of PAN-based precursors to produce carbon fibers more efficiently.

CONCLUSIONS

The successful spinning of PAN fibers containing small concentrations of photoinitiator [4,4′-bis(diethylamino)benzophenone] added externally into the spinning dope (i.e., without incorporating photoinitiators into the polymer chain itself) was demonstrated. It was confirmed that the photoinitiator is retained in the fibers after the coagulation and post-stretching steps. PAN fibers containing 1 wt % photoinitiator showed neither deterioration nor significant morphological differences as compared to pure fibers. Further UV treatment for a short period of time (5 min) of the PAN fibers with 1 wt % photoinitiator led to enhancement of the tensile modulus. Tensile testing results indicated that fibers containing photoinitiator show higher tensile modulus for all set of samples, confirming the positive influence of photoinitiator and further UV treatment in the fibers. This increase of the tensile modulus for fibers containing photoinitiator was largely attributed to the retention of molecular orientation after being UV treated as shown by the WAXD results. These results are very encouraging since the final mechanical properties of the carbon fibers depend greatly on the mechanical properties of the precursor fibers, which in turn, depend on the orientation of the crystals within the fibers. Conversion indices calculated from WAXD spectra prove that the addition of 1 wt % photoinitiator to PAN and UV treatment for only 5 min increases the rate of the cyclization reaction and reduces the thermal oxidation time by over an hour. This could lead to a reduction in the thermal oxidation time while retaining the mechanical properties of the carbon fibers thus produced.

ACKNOWLEDGMENTS

As a subcontractor to Cytec Carbon Fibers, LLC under AFRL Prime Contract No.FA8650-05-D-5807 (AFRL/RXBT Program Monitor: Dr. Karla Strong), Clemson University received partial financial assistance to support this project, which is gratefully acknowledged.

REFERENCES

1. Hou, Y.; Sun, T.; Wang, H.; Wu, D. *J. Appl. Polym. Sci.* **2009**, *114*, 3668.
2. Chen, J.; Ge, H.; Dong, X.; Wang, C. *J. Appl. Polym. Sci.* **2007**, *106*, 692.
3. Catta Preta, I.; Sakata, S.; Garcia, G.; Zimmermann, J; Galembeck, F; Giovedi, C. *J. Therm. Anal. Calorim.* **2007**, *87*, 657.
4. Zhang, W.; Li, M. *J. Mater. Sci. Technol.* **2005**, *21*, 581.
5. Sedghi, A.; Farsani, R.; Shokuhfar, A. *J. Mater. Process. Technol.* **2008**, *198*, 60.
6. Dong, X.; Wang, C.; Chen, J.; Cao, W. *J. Polym. Res.* **2008**, *15*, 125.
7. Jie, L.; Wangxi, Z. *J. Appl. Polym. Sci.* **2005**, *97*, 2047.
8. Mukundan, T.; Bhanu, V. A.; Wiles, K. B.; Johnson, H.; Bortner, M.; Baird, D. G.; Naskar, A. K.; Ogale, A. A.; Edie, D. D.; McGrath, J. E. *Polymer* **2006**, *47*, 4163.
9. Reisch, M. S. *Chem. Eng. News* **2011**, *89*, 10.
10. Gupta, A.; Paliwal, D.; Bajaj, P. *J. Macromol. Sci. Rev. Macromol. Chem. Phys.* **1991**, *C31*, 1.

11. Edie, D. D.; Diefendorf, R. J. In Carbon-Carbon Materials and Composites; Buckley, J. D., Edie, D. D., Eds.; National Aeronautics and Space Administration: Washington, DC, **1992**; Ref. Pub. 1254, Chapter 2, pp 19–39.
12. Shiedlin, A.; Marom, G.; Zilkha, A. *Polymer* **1985**, *26*, 447.
13. Wang, Y.; Wang, Q. *J. Appl. Polym. Sci.* **2007**, *104*, 1255.
14. Yu, M.; Wang, C.; Bai, Y.; Wang, Y.; Zhu, B. *J. Appl. Polym. Sci.* **2006**, *102*, 5500.
15. Wu, G.; Lu, C.; Ling, L.; Hao, A.; He, F. *J. Appl. Polym. Sci.* **2005**, *96*, 1029.
16. Hou, Y.; Sun, T.; Wang, H.; Wu, D. *J. Appl. Polym. Sci.* **2008**, *108*, 3990.
17. Hou, J.; Wang, X.; Zhang, L. *Appl. Phys. Lett.* **2006**, *89*, 152504, 1.
18. Paiva, M. C.; Kotasthane, P.; Edie, D. D.; Ogale, A. A. *Carbon* **2003**, *41*, 1399.
19. Hou, Y.; Sun, T.; Wang, H.; Wu, D. *Text. Res. J.* **2008**, *78*, 806.
20. Mittal, J.; Bahl, O.; Mathur, R. *Carbon* **1997**, *35*, 1196.
21. Wang, Y.; Wang, C.; Bai, Y.; Bo, Z. *J. Appl. Polym. Sci.* **2007**, *104*, 1026.
22. Tan, L.; Pan, J.; Wan, A. *Colloid Polym. Sci.* **2012**, *290*, 289.
23. Wang, P. H. *J. Appl. Polym. Sci.* **1998**, *67*, 1185.
24. Naskar, A. K.; Walker, R. A.; Proulx, S.; Edie, D. D.; Ogale, A. A. *Carbon* **2005**, *43*, 1065.
25. Decker, C. In Photochemistry and Polymeric Systems; Kelly, J. M., Mc Ardle, C. B., Maunder, M. J. de F., Eds.; Royal Society of Chemistry: Cambridge, **1993**; pp 32–46.
26. Endruweit, A.; Johnson, M.; Long, A. *Polym. Compos.* **2006**, *27*, 119.
27. Morales, M.; Ogale, A. *J. Appl. Polym. Sci.* **2013**, *128*, 2081.
28. Ledwith, A. In Photochemistry and Polymeric Systems; Kelly, J. M., Mc Ardle, C. B., Maunder, M. J. de F., Eds.; Royal Society of Chemistry: Cambridge, **1993**; pp 1–14.
29. Fouassier, J. P. *Prog. Org. Coat.* **1990**, *18*, 229.
30. Boyd, I. W.; Zhang, J. Y. *Nucl. Instrum. Methods Phys. Res. B: Beam Inter. Mater. Atoms* **1997**, *121*, 349.
31. Tadmor, Z.; Gogos, C. In Principles of Polymer Processing; Wiley-Interscience Publication: New York, NY, **1979**; Chapter 6, p 146.
32. Middleman, S. In Fundamentals of Polymer Processing; McGraw-Hill, Inc.: New York, NY, **1977**; Chapter 3, p 8.
33. Cullity, B. In Elements of X-Ray Diffraction; Addison-Wesley Publishing Company, Inc.: Reading, MA, **1978**; Chapter 2–9, pp 32–323.
34. Yu, M.; Bai, Y.; Wang, C.; Xu, Y.; Guo, P. *Mater. Lett.* **2007**, *61*, 2292.
35. Dong, X.; Wang, C.; Juan, C. *Polym. Bull.* **2007**, *58*, 1005.
36. Dong, X.; Wang, C.; Bai, Y.; Cao, W. *J. Appl. Polym. Sci.* **2007**, *105*, 1221.
37. Yu, M.; Wang, C.; Bai, Y.; Wang, Y.; Xu, Y. *Polym. Bull.* **2006**, *57*, 757.
38. Peng, G.; Zhang, X.; Wen, Y.; Yang, Y.; Liu, L. *J. Macromol. Sci. Part B: Phys.* **2008**, *47*, 1130.
39. Bashir, Z. *J. Macromol. Sci. Part B: Phys.* **2001**, *40*, 41.
40. Hu, X. *J. Appl. Polym. Sci.* **1996**, *62*, 1925.
41. Zhu, Y.; Wilding, M. A.; Mukhopadhyay, S. K. *J. Mater. Sci.* **1996**, *31*, 3831.
42. Ko, T.; Ting, H.; Lin, C. *J. Appl. Polym. Sci.* **1988**, *35*, 631.
43. Shimada, I.; Takahagi, T. *J. Polym. Sci. Part A: Polym. Chem.* **1986**, *24*, 1989.
44. Sun, T.; Hou, Y.; Wang, H. *J. Appl. Polym. Sci.* **2010**, *118*, 462.
45. Mikolajczyk, T.; Szparaga, G.; Bogun, M.; Fraczek-Szczypta, A.; Blazewicz, S. *J. Appl. Polym. Sci.* **2010**, *115*, 3628.
46. Pinghua, W.; Jie, L.; Zhongren, Y.; Rengyuan, L. *Carbon* **1992**, *30*, 113.
47. Yu, M.; Wang, C.; Bai, Y.; Zhu, B.; Ji, M.; Xu, Y. *J. Polym. Sci. Part B: Polym. Phys.* **2008**, *46*, 759.
48. Matta, V.; Mathur, R.; Bahl, O.; Nagpal, K. *Carbon* **1990**, *28*, 241.
49. Tsai, J.; Hsu, H. *J. Mater. Sci. Lett.* **1992**, *11*, 1403.
50. Sahraoui, B.; Kityk, I.; Kasperczyk, J.; Salle, M.; Nguyen, T. *Opt. Commun.* **2000**, *176*, 503.